Materials Views
www.MaterialsViews.com

ADVANCED MATERIALS INTERFACES
www.advmatinterfaces.de

FULL PAPER

STO/BTO Modulated Superlattice Multilayer Structures with Atomically Sharp Interfaces

Peter K. Petrov, Bin Zou, Yiqian Wang, James M. Perkins, David W. McComb, and Neil McN. Alford*

A comparative study is carried out investigating the microstructure and the electrical properties of $Ba_xSr_{1-x}TiO_3$ films with x = (0.25, 0.5, 0.75) deposited as modulated superlattice (SL) multilayer structures by laser ablation on both $LaAlO_3$ and MgO substrates. The SL structures are examined using high-resolution transmission electron microscopy and scanning transmission electron microscopy. Their interfaces and chemical composition are investigated using energy dispersive X-ray spectroscopy, complemented with electron energy loss spectra analysis performed to give insight to the local chemistry, structure and bonding. It is found that all modulated SL samples consisted of continuous well defined 1 nm $SrTiO_3$ and 4 nm $BaTiO_3$ layers. When modulated SL multilayered structures are compared with their single target deposited equivalents, they exhibit similar electrical properties (e.g. dielectric constant and dielectric loss) but undergo phase transition in a broader temperature region. A very important observation is that the oxygen K-edges in $SrTiO_3$ and $BaTiO_3$ layers are distinctive. Therefore it can be used as finger-print signature for analysis of ultra-thin $SrTiO_3$/$BaTiO_3$ layers and their interfaces. Finally it is demonstrated that by varying the modulation period it is possible to develop structures with engineered ferroelectric properties and improved thermal stability.

1. Introduction

In recent years ultrathin $SrTiO_3$ (STO)/$BaTiO_3$ (BTO) structures have attracted interest[1,2] because of the fundamental scientific importance of their properties[3] (e.g. quasi–two-dimensional electron gases generated at their interfaces)[4] and as a way to fabricate electrically controllable microwave devices[5,6] with enhanced properties.[7,8]

The mutual consensus between all authors investigating such paraelectric, ferroelectric, antiferroelectric, ferromagnetic, or multiferroic, based superlattice (SL) structures both theoretically[9–11] and experimentally[12,13] is that the main reason for their better physical and even unique properties with respect to the parent materials, origins from the microstructure structure of the layers (e.g. residual strain, strain gradient, atoms arrangement etc.) and the quality of their interfaces (defects, dead layers etc).[14] Therefore most of the recent research was devoted to evaluate the relationship between individual SL layers stoichiometry and quality, and the whole structure properties.

The interface quality of the BSTO films and STO/BTO SL structures was studied using high-resolution transmission electron microscopy.[15,16] It was reported that misfit dislocations, threading dislocations, and stacking faults were observed in the single-layered film, while only few threading dislocations were found in the multilayered film. Also, the density of defects in the single-layered film was much higher than in the multilayered film, which was related with the improved thermal stability of the multilayered film. Most recently, Ortega et al.,[12] investigated the lattice distortions to clarify the effect of strain on dielectric and ferroelectric properties of compositionally tailored layers in symmetric BT/(Ba,Sr)TiO_3 SLs.

In[17] it was demonstrated that the strain gradient in STO thin films could be gradually reduced and their electrical properties significantly improved when they were grown as homoepitaxial multilayers using an intermediate oxygen relaxation technique. A pioneering work on development of temperature stable ferroelectric devices was carried out by Gevorgian et al.[18] The principle of the proposed method was to use $Ba_xSr_{1-x}TiO_3$ (BSTO) layers with different barium (Ba) content that have Curie points at different temperatures. By having a bilayer structure where each layer was made of BSTO with different Ba content, the effective operation temperature of the device would be between the Curie temperatures of the two layers. Recently Ortega et al reported[19] a novel application of the BTO/BSTO SLs as high breakdown field and high energy density capacitors in harsh environments; while McMillen et al.[14] by introducing an interfacial dead layer beneath $(BiFeO_3)_{0.6}$-$(SrTiO_3)_{0.4}$ SLs obtained significant improvement in the energy density.

The aim of the present study was to investigate interfaces of modulated STO/BTO SL structures (method 2), and focusing on

Dr. P. K. Petrov, Dr. B. Zou, Dr. J. M. Perkins, Prof. N. M. Alford
Department of Materials, Imperial College London
Prince Consort Road, London, SW7 2AZ, UK
E-mail: p.petrov@imperial.ac.uk
Prof. Y. Q. Wang
Qingdao University
Cultivat Base State Key Lab
Qingdao 266071, China
Prof. D. W. McComb
Department of Materials Science and Engineering
The Ohio State University
Columbus OH 43212, USA

DOI: 10.1002/admi.201300116

 © 2014 WILEY-VCH Verlag GmbH & Co. KGaA, Weinheim

Table 1. Summary of the properties of samples made by both methods.

BSTO Samples	Substrate	Growth Rate Å/pulse	Lattice Parameters, Å			Ba/Sr (EDX)
			a	*b*	*c*	
Target 25/75			**3.931**	**3.931**	**3.931**	**26/74**
Film (method 1)	$LaAlO_3$	0.36	3.927	3.931	3.933	21/79
Film (method 2)	$LaAlO_3$	0.36			3.942	30/70
Target 50/50			**3.955**	**3.955**	**3.951**	**51/49**
Film (method 1)	$LaAlO_3$	0.5	3.965	3.969	3.949	53/47
Film (method 2)	$LaAlO_3$	0.43	3.975	3.986	3.965	58/42
Film (method 1)	MgO	0.53			3.942	55/45
Film (method 2)	MgO	0.48			3.979	58/42
Target 75/25			**3.979**	**3.979**	**3.978**	**75/25**
Film (method 1)	$LaAlO_3$	0.52			3.977	77/23
Film (method 2)	$LaAlO_3$	0.43	3.989	3.995	3.981	80/20

the local chemistry, structure and bonding, to evaluate their effect on the electrical properties of the SL based devices, and compare them with their single target deposited equivalents (method 1).

2. Results and Discussion

Table 1 shows the summary of the properties of all thin films made by both methods. A similar growth rate was used for all samples and the energy dispersive X-ray spectroscopy (EDX) analysis showed that the sample stoichiometry was consistent with that of the target, indicating good stoichiometric mass transfer from the target to the substrate. The compositions achieved by method 1 and method 2 were comparable demonstrating that both methods produce samples with stoichiometry close to that expected.

The X-ray diffraction (XRD) patterns of $Ba_{0.5}Sr_{0.5}TiO_3$ thin films made from both methods on $LaAlO_3$ (LAO) and MgO substrates are shown in **Figure 1**. The patterns demonstrate that both the single and multi-target methods produced single phase epitaxial films with (001) orientation. Slight broadening of the diffraction lines in the films made by method 2 suggests some residual strain is present in the structure. However, it is important to note that the minimal amount of initial BTO and STO phases (traces of BTO and STO were only detected in films thicker than 1 µm). This shows that the thickness of BTO and STO layers does not exceed the critical thickness, *i.e.* their lattices can accommodate the interface mismatch strain through elastic distortion. Furthermore the lattice parameters of the thin films made from both methods are very similar (see Table 1). The slight difference from those of the target can be attributed to substrate/film lattice mismatch and difference in

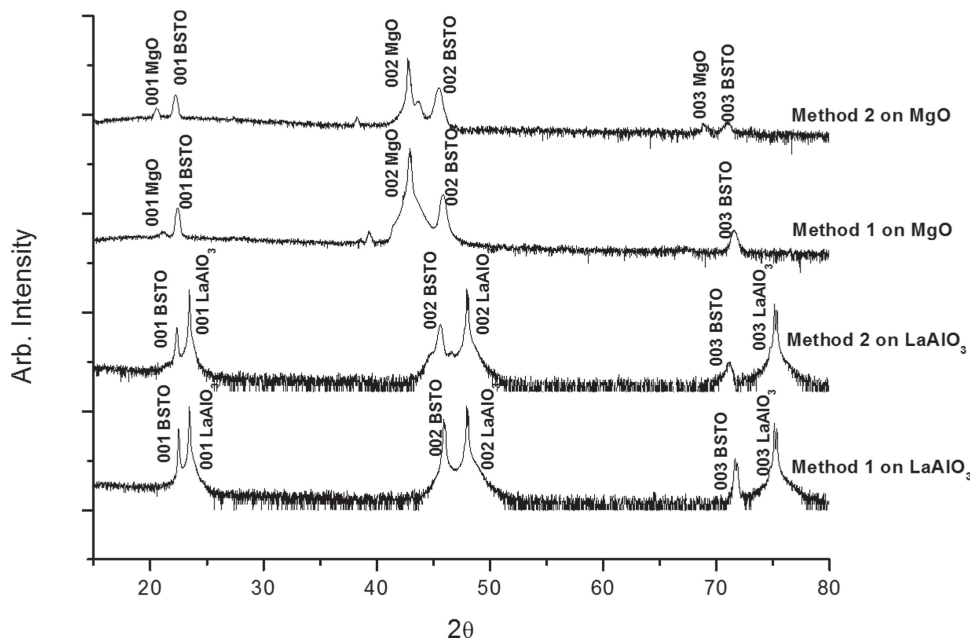

Figure 1. XRD patterns for the films made from single target and multi target $Ba_{0.5}Sr_{0.5}TiO_3$ thin films grown on $LaAlO_3$ and MgO substrates.

© 2014 WILEY-VCH Verlag GmbH & Co. KGaA, Weinheim

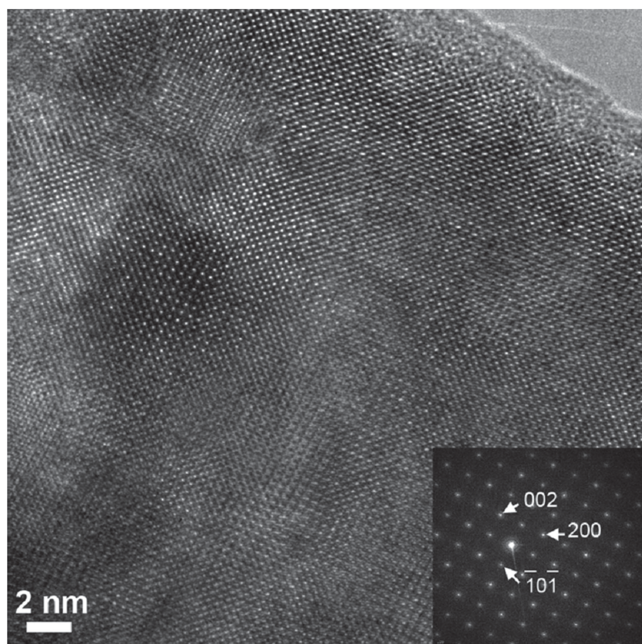

Figure 2. HRTEM image and (inset) SAED of a $Ba_{0.75}Sr_{0.25}TiO_3$ film grown using a single stoichiometric target.

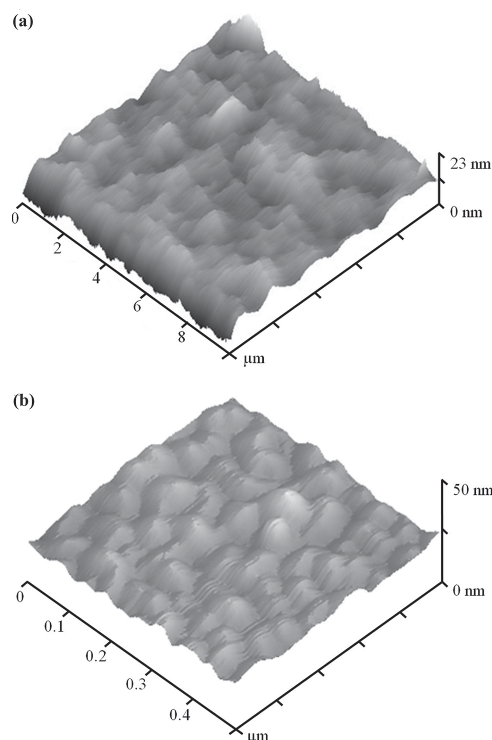

Figure 4. AFM images of the STO/BTO modulated SL structures grown on (a) MgO substrate and (b) $LaAlO_3$ substrate.

their thermal expansion coefficients. (We have to note here that evaluating the in-plane lattice parameters with good accuracy was not always possible, therefore we had to leave some of the boxes in Table 1 empty.)

A typical high resolution transmission electron microscopy (HRTEM) image of a $Ba_{0.75}Sr_{0.25}TiO_3$ film grown using method 1 is shown in **Figure 2**. The film is a high quality single crystal material as evidenced by the selected area electron diffraction pattern (Figure 2). Scanning transmission electron microscopy high angle annular dark field (STEM-HAADF) imaging is often referred to as Z-contrast imaging as the incoherent signal is dominated by Rutherford scattering i.e. is proportional to Z^n (n~2). **Figure 3** shows a typical scanning transmission electron microscopy (STEM) image of the $Ba_{0.75}Sr_{0.25}TiO_3$ thin film grown as modulated SL structure. It clearly demonstrates that well-defined superlattice structure has been grown, with alternating ~4 nm and ~1 nm thick layers, respectively. In the high angle annular dark field (HAADF) image the thicker layers exhibit brighter contrast that the thinner layers which implies that the former are the BTO layers and the latter are the STO layers, which is consistent with the targeted stoichiometry. The modulated STO/BTO SL structure was further confirmed by EDX analysis along the line indicated by an arrow in Figure 3 showing that the minima of the Ba profile corresponds to the maxima of Sr profile extracted from the EDX spectra. These

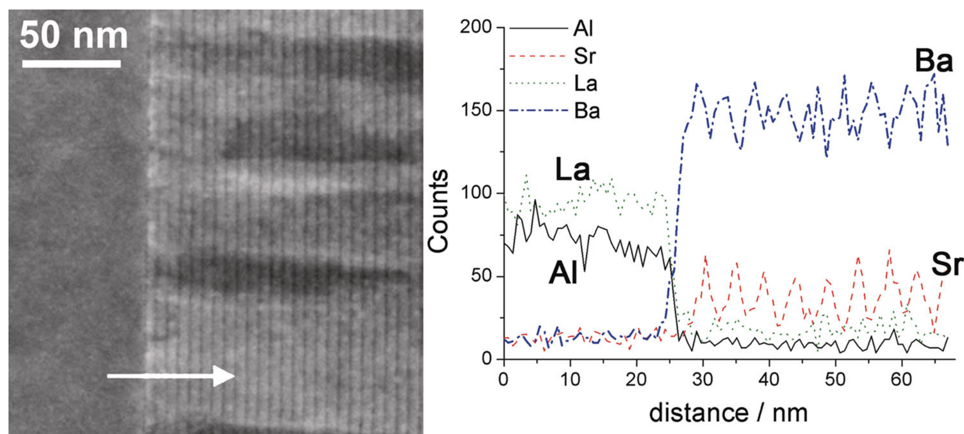

Figure 3. STEM-HAADF image of the STO/BTO multi-layer structure showing the $LaAlO_3$ substrate and BTO/STO multilayers. (STEM probe convergence angle ~14 mrad, HAADF inner collection angle > 77 mrad.) Contrast is due to the atomic number difference between Ba and Sr with Ba layers appearing brighter. EDS line profile position is shown as an arrow on the image.

 © 2014 WILEY-VCH Verlag GmbH & Co. KGaA, Weinheim

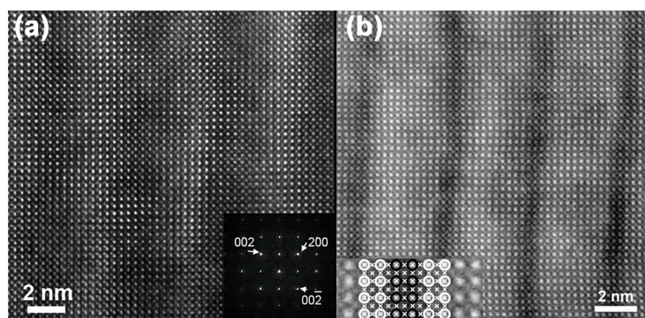

Figure 5. (a) high resolution TEM of a $Ba_{0.75}Sr_{0.25}TiO_3$ film, grown as a multilayered structure. (Inset) the selected area diffraction pattern acquired from within this region of the sample. (b) HR-STEM image of the $Ba_{0.75}Sr_{0.25}TiO_3$ film, grown using a single stoichiometric target showing atomic number contrast between the BTO and STO layers. (Inset) magnified view of the lattice with overlay of Barium and Strontium titanate model structure (black circles Sr columns, white circles Ba columns, x positions indicate Ti and Ti/O columns.) STEM image acquired with a 14mrad convergence angle, and detector inner diameter of >77 mrad.

profiles also show that there is no significant inter-diffusion between the film and the substrate. Columnar defects in the growth direction i.e. perpendicular to the substrate, originate from the twin domain structure of the LAO substrate. These are usually observed in PLD grown films.

The atomic force microscope (AFM) surface analysis showed a RMS (root-mean-square) value of ~2 nm for the SL structure grown on MgO substrate (**Figure 4**a). The RMS value of the structure grown on LAO substrate (Figure 4b) was ~7 nm, which is due to the LAO substrate twinning.

Despite the lattice mismatch between STO and BTO being around 4.8% (a = 3.905 Å and a = 4.100 Å, respectively) no misfit dislocations were observed at the interfaces between BTO and STO layers in the HRTEM (**Figure 5**(a)) and STEM-HAADF images (Figure 5(b)). This confirms that the interface misfit strain is accommodated by the elasticity of the crystal cells. Similar microstructure has been observed in other multilayered systems.[20,21] In the [100] zone axis the brightest spots correspond to the position of the Ba or Sr columns in the perovskite unit cell while the darker spots correspond to the (Ti,O) columns. The inset in Figure 5(b) shows an overlaid schematic of the Ba, Sr and (Ti,O) column positions over a Ba-Sr-Ba interface. Since in essence the metal sub-lattice dominates the contrast, it is possible to observe surface steps at the interfaces between the BTO and STO layers confirming that the PLD growth occurs in a layer-by-layer mode. The HRTEM or phase contrast image cannot be interpreted directly in terms of atomic positions.

Electron energy loss spectroscopy (EELS) was used to analyse the oxygen environment in the BTO and STO layers of the multilayer sample via analysis of the energy-loss near-edge structure (ELNES) on the oxygen K-edge. Previous work on bulk perovskites has demonstrated that the ELNES on the oxygen edge of BTO and STO are different,[22] in particular the peak observed at an energy loss of 545 eV in the STO spectrum splits into two peaks in the spectrum of BTO. In the multilayer sample spectra acquired from the centre of the 1 nm STO layer (spectre 1, **Figure 6**) and the centre of the BTO layer (spectrum 4, Figure 6) are entirely consistent with the data from powdered samples, suggesting that the local oxygen environments are also very similar. Remarkably, spectra acquired at the SL interface from the STO layer side (spectrum 2, Figure 6) and from the BTO layer side (spectrum 3, Figure 6), were entirely consistent with the spectra acquired from the middle of the STO and BTO layers, respectively. This is a significant result demonstrating the sharp, defect free interface between the films of the SL structure. It is also important to note the appearance of

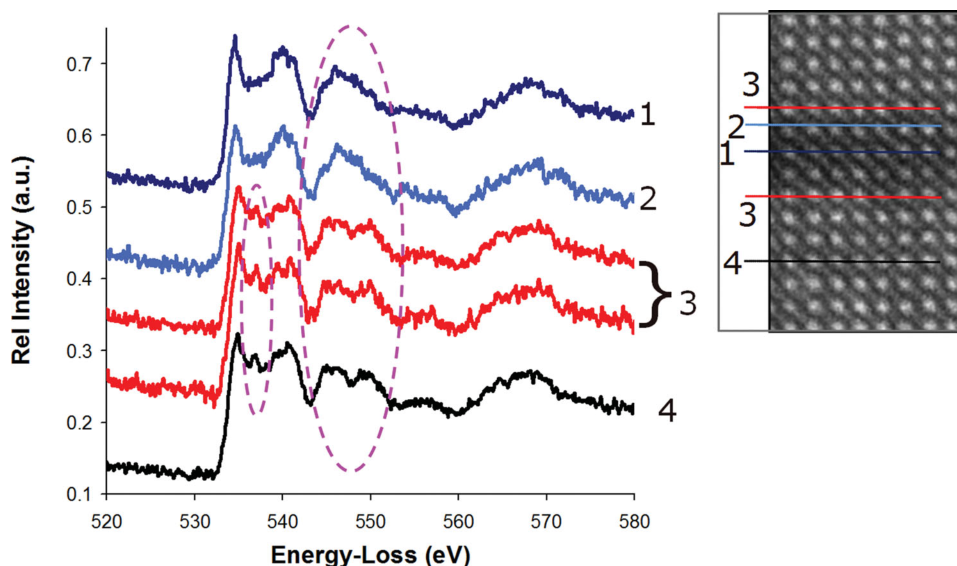

Figure 6. Electron energy loss (EEL) spectra acquired from BTO and STO layers showing the oxygen (K) near-edge structure. (STEM-EELS 14 mrad convergence, 20 mrad collection angle). Numbered lines in the insert show the spectra acquisition directions: 1 – in the middle of the STO layer, 2 – near the interface of the STO layer, 3 – near the interface of the BTO layer, 4 – in the middle of the BTO layer. The dashes ellipses highlight the split into two peaks (energy loss of 545 eV) and appearance of an extra peak (energy loss of 537 eV) in the BTO spectra.

© 2014 WILEY-VCH Verlag GmbH & Co. KGaA, Weinheim

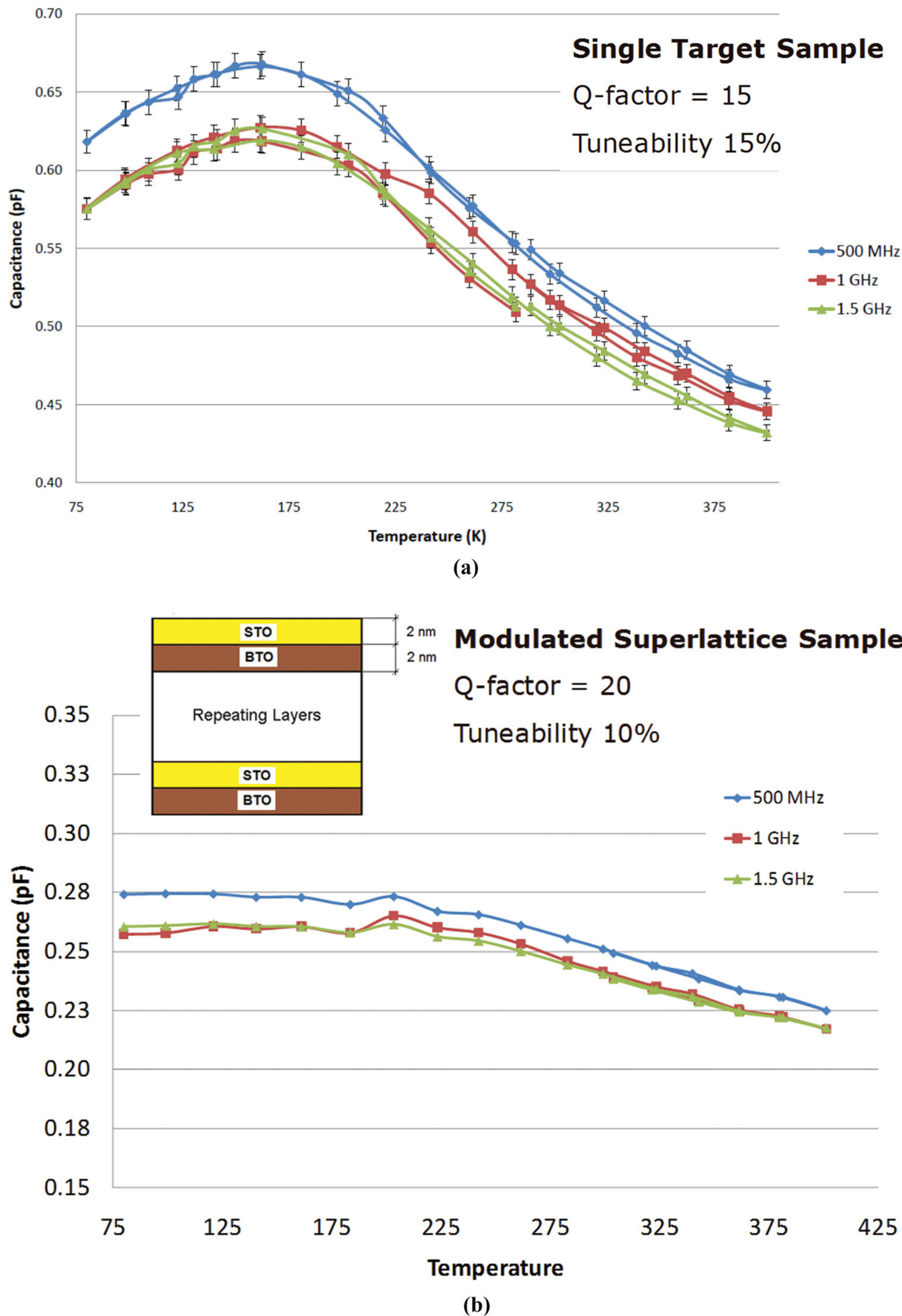

Figure 7. Temperature dependences of the of $Ba_{0.5}Sr_{0.5}TiO_3$ samples made using method 1 (a) and method 2 (b).

an extra peak (energy loss of 537 eV) in the BTO spectra. This peak was not observed the spectrum acquired from the powdered samples and therefore it can be used as a "finger-print" signature for analysis of ultra-thin $SrTiO_3/BaTiO_3$ layers and their interfaces.

Typical results of the microwave measurements performed in a temperature range (100 K – 400 K) are presented in **Figure 7**. Comparing both structures one can note: (i) the difference in the capacitance value, which can be associated with the residual strain/space charge induced polarization at the SL interfaces[23] and the inhomogeneous electromagnetic field distribution in the modulated SL sample; (ii) frequency dependence of the capacitance value, which is gradually reduced in the modulated SL sample. The frequency dependence of a capacitor structure is usually caused by the leakage current, and its reduction manifests improvement of the

© 2014 WILEY-VCH Verlag GmbH & Co. KGaA, Weinheim

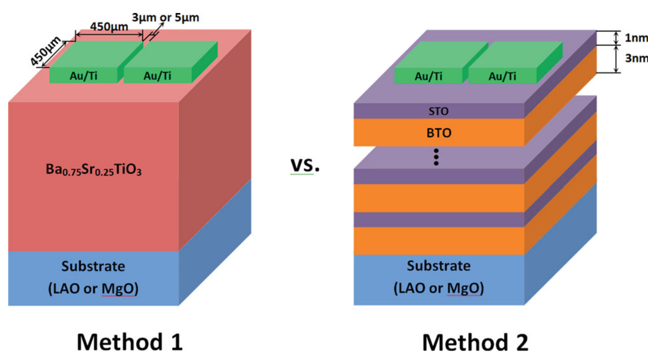

Figure 8. Sample deposition methods: Method 1 – using single stoichiometric BSTO target and Method 2 – using two targets of STO and BTO.

dielectric properties of the structure. (iii) One can also note the improved temperature dependence of the capacitor based on the modulated SL structure (Method 2). This is because the elastically accommodated interface strain broadens both STO and BTO layers transition temperatures resulting in a near linear temperature dependence over a wide temperature range. This result is in good agreement with,[12] where the authors observed no phase transition in their STO/BTO symmetric SL structure. Finally, the compressive (*in-plane*) residual strain in the BTO layer is also responsible for the slight reduction of the electrical tunability (defined as $n = (C(0V) - C(V_{max)})/C(0V))$ of the modulated SL structure capacitor, while the increase of the Q-factor is due to the influence of the low loss STO layer on the enhanced SL sample.

3. Conclusion

A comparative study was carried out investigating the microstructure and the electrical properties of $Ba_xSr_{1-x}TiO_3$ films with x = (0.25, 0.5, 0.75) deposited as modulated SL multilayer structures by laser ablation on both $LaAlO_3$ and MgO substrates. The SL structures were investigated using high-resolution transmission electron microscopy and scanning transmission electron microscopy**.** The SL interfaces and chemical composition were investigated using energy dispersive X-ray spectroscopy, and with electron energy loss spectra analysis performed to give insight to the local chemistry, structure and bonding. It was found that all modulated SL samples consisted of continuous well defined 1 nm $SrTiO_3$ and 4 nm $BaTiO_3$ layers. When modulated SL based capacitor structures were compared with their single target deposited equivalents, they exhibited similar electrical properties (e.g. dielectric constant and dielectric loss) but underwent phase transition in a broader temperature region.

A very important observation was that the oxygen K-edges in STO and BTO layers are distinctive. Therefore they can be used as finger-print signatures for analysis of ultra-thin $SrTiO_3/BaTiO_3$ layers and their interfaces.

Finally it was demonstrated that by varying the modulation period it is possible to fabricate BSTO thin films with engineer Ba/Sr stoichiometric ratio, and therefore develop both high power and high energy density dielectric devices with improved thermal stability.

4. Experimental Section

A set of $Ba_xSr_{1-x}TiO_3$ (where x = 0.25, 0.50 and 0.75) thin films were deposited on $LaAlO_3$ and MgO substrates using a single stoichiometric BSTO target (method 1). Another set of samples with the same stoichiometry were deposited as a periodic superlattice of BTO and STO layers (method 2) (**Figure 8**). The stoichiometry in the modulated superlattice sample was controlled by varying the relative thickness of the STO and BTO layers, ensuring that the layer thickness did not exceed the critical thickness required for epitaxial growth. All samples were made under same conditions, maintaining the same total number of laser pulses.

Targets for the PLD system were made from ceramic powder prepared using the mixed oxide route.[24,25] Thin films were grown by laser ablation (Neocera PLD system with a Lambda Physik KrF laser, $\lambda = 248$ nm) on epi-polished, 5 × 5 mm^2 $LaAlO_3$ and MgO substrates, secured by silver paste onto the stainless-steel resistive heater with a target to substrate distance of 50 mm. The $LaAlO_3$ substrates were not specially treated (e.g. terminated) as the previous studies reported contradicting results about the effect of the $LaAlO_3$ single crystal surface termination[26] and its high temperature stability.[27] Thin films were deposited from 20 mm diameter stoichometric $BaTiO_3$, $SrTiO_3$, and $Ba_xSr_{1-x}TiO_3$ targets in an oxygen pressure of 300 mTorr. The substrate temperature (T_s = 740 K) during deposition was controlled using a thermocouple embedded in the heater. The energy density of the laser spot (2 × 10 mm^2) was 2.5 J/cm^2. From the sample thickness measured using a Dektak 11A, the film growth rate was estimated to be approximately 0.05 nm/pulse. The total number of pulses was 5000 with a repetition rate of 8 Hz. Once the ablation was over, the samples were then cooled down at a rate of 10 °C/min in an oxygen rich environment (760 Torr).

All samples were examined by conventional X-ray diffraction on a PAnalytical X'Pert MRD system. In-plane lattice parameters were examined using grazing-incidence X-ray diffraction.[28,29] The stoichiometry of the sample (targets and thin films) was examined by EDX using an Oxford Instruments INCA system attached to a Hitachi 4300 field-emission-gun SEM. A Veeco (Bruker) AFM was used for investigation of the samples surface.

HRTEM and STEM-HAADF imaging as well as the chemical analysis were carried out using an FEI Titan 80/300 scanning transmission electron microscope. Chemical analysis was performed using EDX and EELS. A monochromator on the electron source allowed an energy resolution in EELS better than 0.2 eV to be achieved. TEM samples were prepared using the conventional cross section method[30] and focused ion beam (FEI Nova dual beam FIB) *in-situ* lift out. Samples prepared by both methods underwent final stage low energy (0.2 – 0.5 kV) ion milling. All samples were plasma cleaned for 1 minute using an Ar/O_2 gas mixture to remove contamination prior to inserting in the microscope.

For electrical testing, planar-capacitor structures with 3 µm and 5 µm gap-size were patterned on the film surface: 0.5 µm thick Au/Ti electrodes were formed using E-beam evaporation followed by photolithography and ion-milling performed on an Oxford Applied Research OAR–IM150 system.

Electrical measurements in a temperature range between 100 K and 400 K were performed on a Janis Inc. cryo- probe station. An Agilent 4287A RF LCR meter was used for direct measurement of the sample capacitance and Q-factor. GGB Picoprobes and Suss Microtek IZI probes were used in these measurements.

Acknowledgements

This work was financially supported by the UK Engineering and Physical Sciences Research Council (EPSRC).

Received: November 18, 2013
Revised: January 17, 2014
Published online: March 28, 2014

© 2014 WILEY-VCH Verlag GmbH & Co. KGaA, Weinheim

[1] D. A. Tenne, A. Bruchhausen, N. D. Lanzillotti-Kimura, A. Fainstein, R. S. Katiyar, A. Cantarero, A. Soukiassian, V. Vaithyanathan, J. H. Haeni, W. Tian, D. G. Schlom, K. J. Choi, D. M. Kim, C. B. Eom, H. P. Sun, X. Q. Pan, Y. L. Li, L. Q. Chen, Q. X. Jia, S. M. Nakhmanson, K. M. Rabe, X. X. Xi, *Science* **2006**, *313*, 1614.
[2] E. Bousquet, M. Dawber, N. Stucki, C. Lichtensteiger, P. Hermet, S. Garilio, J-M. Triscone, P. Ghosez, *Nature* **2008**, *452*, 732–736.
[3] D. D. Fong, G. B. Stephenson, S. K. Streiffer, J. A. Eastman, O. Auciello, P. H. Fuoss, C. Thompson, *Science* **2004**, *304*, 1650–1653.
[4] S. Thiel, G. Hammerl, A. Schmehl, C. W. Schneider, J. Mannhart, *Science* **2006**, *313*, 1942.
[5] M. J. Lancaster, J. Powell, A. Porch, *Supercond. Sci. Technol.* **1998**, *11*, 1323.
[6] A. K. Tagantsev, V. O. Sherman, K. F. Astafiev, J. Venkatesh, N. Setter, *J. Electrocer.* **2003**, *11*, 5.
[7] M. Stengel, D. Vanderbilt, N. A. Spaldin, *Nat. Mater.* **2009**, *8*, 392.
[8] S. S. Spartak, E. L. Kollberg, *IEEE Trans. Microwave Theory Technol.* **2001**, *49*(11), 2117.
[9] H. N. Lee, H. M. Christen, M. F. Chisholm, C. M. Rouleau, D. H. Lowndes, *Nature* **2005**, *433*, 395.
[10] J. Lee, L. Kim, J. Kim, D. Jung, U. V. Waghmare, *J. Appl. Phys.* **2006**, *100*, 051613.
[11] K. Rogdakis, J. W. Seo, Z. Viskadourakis, Y. Wang, L. F. N. Ah Qune, E. Choi, J. D. Burton, E. Y. Tsymbal, J. Lee, C. Panagopoulos, *Nat. Commun.* **2012**, *3*, 1064.
[12] N. Ortega, A. Kumar, O. Resto, O. A. Maslova, Y. I. Yuzyuk, J. F. Scott, R. S. Katiyar, *J. Appl. Phys.* **2013**, *114*, 104102.
[13] G. Panomsuwan, O. Takai, N. Saito, *Appl. Phys. Lett.* **2013**, *103*, 112902.
[14] M. McMillen, A. M. Douglas, T. M. Correia, P. M. Weaver, M. G. Cain, J. M. Gregg, *Appl. Phys. Lett.* **2012**, *101*, 242909.
[15] Y. Q. Wang, W. S. Liang, P. K. Petrov, N. Alford, *Mater. Charact.* **2011**, *62*, 294.
[16] Y. Q. Wang, W. S. Liang, P. K. Petrov, N. Alford, *Appl. Phys. Lett.* **2011**, *98*, 091910.
[17] P. K. Petrov, N. Alford, *Appl. Phys. Lett.* **2005**, *87*, 222902.
[18] S. S. Gervorgian, P. K. Petrov, Z. Ivanov, E. Wilkborg, *App Phys Lett.* **2001**, *79*, 1861.
[19] N. Ortega, A. Kumar, J. F. Scott, D. B. Chrisey, M. Tomazawa, S. Kumari, D. G. B. Diestra, R. S. Katiyar, *J. Phys.: Condens. Matter.* **2012**, *24*, 445901.
[20] J. C. Jiang, X. Q. Pan, W. Tian, C. D. Theis, D. G. Schlom, *Appl. Phys. Lett.* **1999**, *74*, 2851.
[21] T.-U. Kim, B. R. Kim, W.-J. Lee, J. H. Moon, B.-T. Lee, J. H. Kim, *J. Cryst. Growth* **2006**, *289*, 540.
[22] P. Harkins, D. W. McComb, M. MacKenzie, A. J. Craven, *Inst. Phys. Conf. Ser.* **2004**, *179*, 119.
[23] A. Q. Jiang, J. F. Scott, M. Dawber, C. Wang, *J. Appl. Phys.* **2002**, *92*, 6756.
[24] G. H. Haertling, *J. Am. Ceram. Soc.* **1999**, *82*(4) 797.
[25] K. Sarma, R. Farooq, K. Jarman, R.C. Pullar, P. K. Petrov, N. M. Alford, *Integr. Ferroelectr.* **2004**, *62*, 249.
[26] M. Huijben, A. Brinkman, G. Koster, G. Rijnders, H. Hilgenkamp, D. Blank, *Adv. Mater.* **2009**, *21*, 1665.
[27] Z. Q. Liu, Z. Huang, W. M. Lu, K. Gopinadhan, X. Wang, A. Annadi, T. Venkatesan, Ariando, *AIP Adv.* **2012**, *2*, 012147.
[28] P. K. Petrov, K. Sarma, N. M. Alford, *Integr. Ferroelectr.* **2004**, *63*, 183.
[29] P. K. Petrov, Z. G. Ivanov, S. S. Gevorgyan, *Mater. Sci. Eng.* **2000**, *A288*, 231.
[30] C. P. Scott, A. J. Craven, P. Hatto, C. Davies, *J. Microsc.* **2003**, *182*, 186.

© 2014 WILEY-VCH Verlag GmbH & Co. KGaA, Weinheim